Thermal Expansion of the Superhydrated Small-Pore Zeolite Natrolite

ARTICLE *in* THE JOURNAL OF PHYSICAL CHEMISTRY C · FEBRUARY 2012

Impact Factor: 4.77 · DOI: 10.1021/jp209514q

THE JOURNAL OF PHYSICAL CHEMISTRY C

Article

pubs.acs.org/JPCC

Thermal Expansion of the Superhydrated Small-Pore Zeolite Natrolite

Yongjae Lee,*[,†] Chi-Chang Kao,[‡] and Thomas Vogt[§]

[†]Department of Earth System Sciences, Yonsei University, Seoul 120-749, Korea

[‡]Stanford Synchrotron Radiation Lightsource, SLAC National Accelerator Laboratory, Menlo Park, California 94025-7015, United States

[§]NanoCenter & Department of Chemistry and Biochemistry, University of South Carolina, Columbia, South Carolina 29208, United States

ABSTRACT: Natrolite ($Na_{16}Al_{16}Si_{24}O_{80}\cdot16H_2O$) at ambient conditions is *the* paradigmatic example of an auxetic material whose behavior under pressure can be rationalized using a "rotating squares" model with the squares being made up of T_5O_{10} subunits (T = Al, Si). This model also rationalizes reversible superhydration where water is inserted under pressure ("pressure-induced hydration"). Using combined pressure and temperature in situ synchrotron powder diffraction techniques, we have investigated the structural changes occurring in "superhydrated" natrolite ($Na_{16}Al_{16}Si_{24}O_{80}\cdot32H_2O$) between 20 and 300 K at 1.7(3) GPa. Rietveld refinements allowed us to identify significant changes within the sodium–water substructure located in the pores of the superhydrated natrolite. Despite the higher water content of the superhydrated phase, its thermal volumetric expansion coefficient is 15 times larger than that of natrolite at ambient pressure. We put forward a structural descriptor relating thermal expansion and the rotations of T_5O_{10} units that measures the impact of nonframework cations and water contained in the pores on the "rotational squares" mechanism.

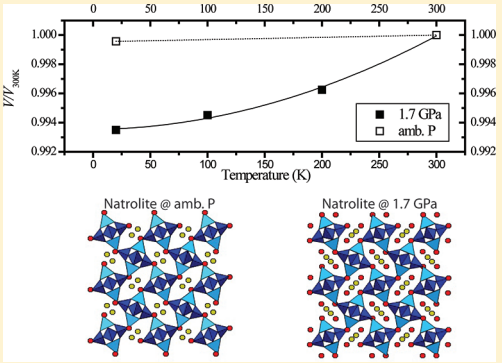

INTRODUCTION

Recent interest in the high-pressure chemistry of zeolites and other microporous materials arose due to the discovery of the pressure-induced hydration (PIH) observed in the aluminosilicate natrolite, $Na_{16}Al_{16}Si_{24}O_{80}\cdot16H_2O$, and its synthetic gallosilicate analogues.[1−6] Pressure-induced hydration leads to the formation of "superhydrated" materials under hydrostatic pressure, i.e., $Na_{16}Al_{16}Si_{24}O_{80}\cdot32H_2O$, which contain more water within their micropores than the initial materials at ambient pressure, i.e., $Na_{16}Al_{16}Si_{24}O_{80}\cdot16H_2O$.

The natrolite framework is composed of T_5O_{10} (T = Si, Al, Ga, Ge...) tetrahedral units, which in the case of natrolite have a SiO_4 tetrahedron as a central polyhedron and the surrounding two SiO_4 and two AlO_4 tetrahedra in alternation to satisfy the Loewenstein rule.[7] The T_5O_{10} units are then connected along the *c*-axis, forming the so-called natrolite chains.[8,9] The 2_1 screw axis of the *Fdd2* (orthorhombic) space group reproduces the T_5O_{10} units, creating helical eight-ring channels along the *c*-axis with $T_{10}O_{20}$ windows intersecting perpendicular to the channel (see Figures 1a and b).

An angular distortion parameter, ψ, defined as the average of $\psi1$ and $\psi2$ (see Figures 1a and 1b) measuring the average angle between the sides of the quadrilateral around the T_5O_{10} secondary building unit and the *a*- and *b*-unit cell axes, quantifies the degree of chain rotation.[10] The smaller this ψ angle is, the more circular the helical eight-ring window becomes and the easier access to the channel will be for small atoms and molecules such as H_2O, Ar, and CO_2 (see Figure 1b).[3,11,12] PIH of natrolite first gives rise to an ordered-paranatrolite phase[3] ($Na_{16}Al_{16}Si_{24}O_{80}\cdot24H_2O$) and subsequently at higher pressures to a fully superhydrated natrolite[4] ($Na_{16}Al_{16}Si_{24}O_{80}\cdot32H_2O$). When subjected to hydrostatic conditions in the presence of water, natrolite ($Na_{16}Al_{16}Si_{24}O_{80}\cdot16H_2O$), which has one water molecule per sodium, shows an abrupt volume expansion of ca. 7% near 1.0(1) GPa and afterward a contraction of ca. 4% at pressures above 1.2(1) GPa.[3,4] These unit cell volume changes are due to the successive and selective uptake of water molecules from the water-containing pressure-transmitting media through the eight-ring window. In the initial stages of PIH, the eight-ring window becomes more circular as the ψ angle decreases from 24.0(1)° to 20.7(1)°. This allows the insertion of eight additional water molecules per formula unit at 1.0(1) GPa[3] and the formation of an ordered-paranatrolite phase with the formula $Na_{16}Al_{16}Si_{24}O_{80}\cdot24H_2O$. Further increasing the pressure leads to the window becoming more elliptical as the ψ angle expands to 23.7(1)° above 1.2(1) GPa. This results in the formation of superhydrated natrolite, which contains two water molecules per sodium ion, with the formula

Received: October 3, 2011
Revised: January 5, 2012
Published: January 9, 2012

   dx.doi.org/10.1021/jp209514q | *J. Phys. Chem. C* 2012, 116, 3286–3291

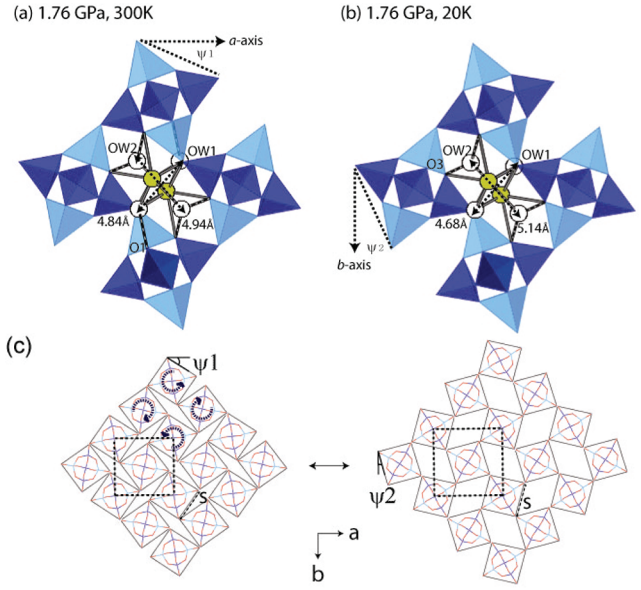

Figure 1. Polyhedral representations of superhydrated natrolite at 1.7(3) GPa at (a) 300 K and (b) 20 K, viewed along the chain/channel axis. Filled circles represent sodium cations; open circles water oxygen atoms. Silicon and aluminum tetrahedra are shown in dark and light colors, respectively, to illustrate their ordering over the framework tetrahedral sites. Filled lines around the sodium atoms illustrate Na−O and Na−H_2O coordination, and dotted lines around the water oxygen atoms show bonding to the framework oxygen atoms. The chain rotation angle, ψ, is an average of $\psi 1$ and $\psi 2$, which are depicted with respect to a T_5O_{10} building unit and the appropriate axis. (c) Shown is the concerted rotational behavior of the framework occurring in the plane perpendicular to the channel *c*-axis ("rotating squares" model). Each square net represents a dense T_5O_{10} unit, composed of Si (blue) and Al (cyan) tetrahedra, connected by oxygen (red) "hinges". The channel opening is defined by the chain rotation angle (ψ) and the rigid T_5O_{10} unit edge length (s). Dotted lines show 2D unit cells, and arrows indicate the cooperative chain rotation.

$Na_{16}Al_{16}Si_{24}O_{80}{\cdot}32H_2O$.[3,4] More details about the structural changes during PIH are given in reference 3.

Besides water, other molecules and atoms can also be inserted into natrolite under pressure. The structural changes as indicated by the opening of the eight-ring window are remarkably similar: in the case of argon insertion an average composition of $Na_{16}Al_{16}Si_{24}O_{80}{\cdot}16H_2O{\cdot}0.6Ar$ was observed near 3 GPa with a ψ angle of 20.4(1)°,[11] very close to the 20.7(1)° observed in the $Na_{16}Al_{16}Si_{24}O_{80}{\cdot}24H_2O$ paranatrolite phase. The insertion of CO_2 molecules into natrolite at 1.5 GPa and 110 °C results in the formation of $Na_{16}Al_{16}Si_{24}O_{80}{\cdot}16H_2O{\cdot}8CO_2$ with a ψ angle of 20.5(1)°.[12]

At ambient conditions, natrolite thus has an ordered distribution of Al and Si located on the T-sites in *Fdd*2 symmetry and sodium cations sited along the channels and water molecules situated close to the $T_{10}O_{20}$ windows. The water molecules are located on the 16b site in *Fdd*2, creating 16 crystallographically equivalent water molecules per unit cell.[8] Early neutron diffraction studies[13] as well as Raman and IR spectroscopic investigations[14] of $Na_{16}Al_{16}Si_{24}O_{80}{\cdot}16H_2O$ at ambient pressure indicate that one of the two hydrogen atoms of the water molecule located in the pore is shorter and more strongly hydrogen bonded to the framework oxygen and located in the *bc*-plane, while the other longer and weaker hydrogen-bonded one is located in the *ac*-plane. The O−H stretching modes of water, the mode near 3320 cm^{-1} for the strong hydrogen bond, and the other one near 3540 cm^{-1} assigned to the weaker hydrogen bond vary in opposite ways as the temperature is lowered; i.e., the mode at 3320 cm^{-1} decreases, whereas the one at 3540 cm^{-1} increases. The magnitude of the change is about the same. This indicates that there is no or very little change in the strength of the hydrogen bonding of the water as a function of temperature in $Na_{16}Al_{16}Si_{24}O_{80}{\cdot}16H_2O$ at ambient pressure.[14]

The results of in situ high-pressure neutron powder diffraction[15,16] provided some details of the structural changes that accompanied the water insertion during PIH as the eight-ring window opens: the original water molecules ("type-1 water") present at ambient conditions continue to be bonded via hydrogen bonds to the oxygen of the natrolite framework as described above. The water molecules inserted under pressure are located on the 16b site in the space group *Fdd*2 and describe 16 equivalent water molecules within the unit cell. We will refer to them as "type-2 water molecules". They also form hydrogen bonds to oxygen of the natrolite framework, albeit much weaker. These type-1 and type-2 water molecules in superhydrated $Na_{16}Al_{16}Si_{24}O_{80}{\cdot}32H_2O$ engage in no direct hydrogen bonding with each other, contrary to earlier speculations.[17] Furthermore, while the type-1 water molecules are coordinated to two sodium atoms, the type-2 ones are only bonded to one sodium and as a result are significantly underbonded.[15] This difference of the water coordination can be a reason why PIH in natrolite is a reversible process and the type-2 water molecules are expelled from the channels at lower pressures. The structural changes during PIH as deduced from our extensive crystallographic studies on natrolites[2−5,18,19] reveal that under pressure the channels through which water can diffuse open up due to the antirotation of the T_5O_{10} units composed of corner-sharing SiO_4 and AlO_4 tetrahedra connected by oxygen "hinges" (Figure 1). Baur[20,21] categorized these flexible frameworks as either "collapsible" or "non-collapsible" depending on whether the hinges corotate in the same (collapsible) or as in natrolite in the opposite (non-collapsible) directions. Such a "rotating squares" mechanism[24] based on rigid tetrahedral units and "soft hinges" leading to a pore and volume expansion and concomitant pressure-induced hydration has been independently discussed in the literature as one of the ways that auxetic behavior of materials manifests itself at the atomistic scale.[22,23] An auxetic material has negative Poisson's ratios leading to a thinning of material when compressed or an expansion when stretched in a perpendicular direction.[24,25] Figure 1c depicts how the counter rotations of the T_5O_{10} units open up the eight-ring windows and allow for the penetration of molecules under pressure. This simple rotating squares model relates PIH and other pressure-induced adsorption processes to the auxetic properties. Recently, Grima et al.[26] showed experimentally that natrolite is indeed an auxetic zeolite with negative Poisson ratios providing thus corroboration for a model to rationalize pressure-induced hydration in natrolite.

Thermal expansion provides important insights into the framework flexibility and dynamics of zeolitic materials. It has been argued that water and nonframework cations located within the pores of natrolite have an important influence on auxetic properties by impeding the rotations of the T_5O_{10} units.[27,28] The temperature-dependent structural changes of a superhydrated zeolite have not been investigated up to now. Our results are important to compare with modeling results

dx.doi.org/10.1021/jp209514q | J. Phys. Chem. C 2012, 116, 3286−3291

Table 1. Final Refined Atomic Coordinates for the Superhydrated Natrolite at 1.76 GPa and Different Temperatures[a]

pressure, temperature		1.76 GPa, 20 K	1.76 GPa, 100 K	1.76 GPa, 200 K	1.76 GPa, 300 K
space group		*Fdd*2	*Fdd*2	*Fdd*2	*Fdd*2
$_wR_p$ (%), χ^2		2.10, 6.68	2.07, 4.95	2.01, 4.39	1.75, 2.53
cell lengths (Å)	*a*	18.267(1)	18.279(1)	18.3172(9)	18.3841(8)
	b	18.783(1)	18.792(1)	18.7996(9)	18.8192(9)
	c	6.5573(4)	6.5564(4)	6.5516(3)	6.5455(3)
cell volume (Å^3)	*V*	2249.8(3)	2252.1(2)	2256.1(2)	2264.6(2)
Si(1), *8a*	*x*	0.0000	0.0000	0.0000	0.0000
	U_{iso} [b]	0.009(1)	0.009(1)	0.005(1)	0.021(1)
Si(2), *16b*	*x*	0.1525(2)	0.1538(4)	0.1529(4)	0.1535(3)
	y	0.2116(2)	0.2096(4)	0.2103(3)	0.2100(3)
	z	0.6174(4)	0.6184(9)	0.6174(9)	0.6181(7)
Al, *16b*	*x*	0.0397(2)	0.0415(4)	0.0406(4)	0.0397(3)
	y	0.0935(2)	0.0930(4)	0.0926(3)	0.0933(3)
	z	0.6103(4)	0.6118(9)	0.6110(9)	0.6099(7)
O(1), *16b*	*x*	0.0392(4)	0.0414(5)	0.0393(5)	0.0386(5)
	y	0.0597(3)	0.0587(4)	0.0603(4)	0.0601(3)
	z	0.8590(4)	0.8603(10)	0.8617(10)	0.8596(8)
O(2), *16b*	*x*	0.0693(2)	0.0701(4)	0.0699(4)	0.0707(3)
	y	0.1820(2)	0.1818(4)	0.1811(3)	0.1811(3)
	z	0.6080(7)	0.6065(18)	0.6046(17)	0.6063(13)
O(3), *16b*	*x*	0.0979(3)	0.0988(6)	0.0990(5)	0.0971(5)
	y	0.0416(2)	0.0393(4)	0.0394(4)	0.0394(3)
	z	0.4593(10)	0.4631(16)	0.4652(16)	0.4635(13)
O(4), *16b*	*x*	0.2005(2)	0.2026(4)	0.2023(4)	0.2015(3)
	y	0.1599(3)	0.1582(5)	0.1587(5)	0.1570(4)
	z	0.7628(9)	0.7625(16)	0.7594(15)	0.7591(13)
O(5), *16b*	*x*	0.1884(3)	0.1892(4)	0.1881(4)	0.1888(4)
	y	0.2124(4)	0.2113(5)	0.2129(5)	0.2123(5)
	z	0.3915(4)	0.3915(11)	0.3906(10)	0.3914(8)
Na, *16b*	*x*	0.2303(8)	0.2305(7)	0.2298(7)	0.2272(7)
	y	0.0209(7)	0.0216(7)	0.0200(6)	0.0190(6)
	z	0.604(3)	0.606(3)	0.611(3)	0.609(3)
OW1, *16b*	*x*	0.061(1)	0.062(1)	0.0632(9)	0.064(1)
	y	0.184(1)	0.185(1)	0.1822(9)	0.179(1)
	z	0.124(6)	0.119(7)	0.118(6)	0.118(6)
OW2, *16b*	*x*	0.176(1)	0.178(1)	0.176(1)	0.181(1)
	y	0.077(1)	0.076(1)	0.077(1)	0.072(1)
	z	0.111(3)	0.116(4)	0.101(3)	0.101(4)

[a]Esd's are in parentheses. [b]Isotropic displacement parameters, U_{iso}, are constrained to be the same for all atoms. All the sites are fully occupied.

probing auxetic behavior and enhance our understanding of superhydrated phases. Here, we report on the structural changes of superhydrated natrolite using temperature-dependent synchrotron powder diffraction measurements at 1.7(3) GPa.

EXPERIMENTAL SECTION

In situ combined high-pressure and low-temperature synchrotron X-ray powder diffraction experiments were performed at the X7A beamline at the National Synchrotron Light Source (NSLS) at Brookhaven National Laboratory (BNL). The primary white beam from the bending magnet was focused in the horizontal plane using a triangular Si(111) monochromator bent to a cylindrical curvature by applying a load to the crystal tip, creating a ~200 μm focal spot of monochromatic X-rays with a wavelength of 0.6545 Å. A gas-proportional position-sensitive detector (PSD) gated on the Kr-escape peak was used to collect high-resolution powder diffraction data ($\Delta d/d \sim 10^{-3}$).[29] The PSD covered 4° in 2θ and was stepped in 0.25° intervals over the angular range of 3.5−35.5° with counting times of 90−150 s per step. The wavelength of the incident beam was determined from a CeO_2 standard (SRM 674).

A modified Merrill-Bassett diamond anvil cell (DAC) was used as the pressure vessel, equipped with two type-I diamond anvils (culet diameter of 700 μm) and tungsten-carbide supports.[30] A stainless-steel foil of 250 μm thickness was preindented to a thickness of about 100 μm, and a 250 μm hole was obtained by electro-spark erosion. A powdered sample of the mineral natrolite, identical to that used in our previous high-pressure studies,[3,4] was loaded in the DAC along with ruby chips and some NaCl for a combined pressure−temperature calibration at ambient and low-temperature conditions, respectively. A drop of a methanol:ethanol:water (16:3:1 by volume) mixture was then added to the sample chamber as a hydrostatic pressure-transmitting medium.[31] The sample pressure was gradually increased at room temperature until the formation of the superhydrated natrolite was identified by XRD at 1.7(3) GPa. The DAC was then placed inside a closed-cycle He cryostat and cooled to 20 K. Synchrotron X-ray powder diffraction data were collected at 20, 100, 200, and 300

dx.doi.org/10.1021/jp209514q | J. Phys. Chem. C 2012, 116, 3286−3291

K. At each temperature point, the NaCl lattice constant was determined, and the pressure was determined using the equation of state of NaCl.[32] Full pattern LeBail fitting was used to determine an accurate value of the NaCl lattice parameter, which revealed that the pressure drift caused by cooling the DAC is ca. 0.2 GPa.

The structural refinements of the superhydrated natrolite at low temperature were performed with Rietveld methods using the GSAS suite of programs.[33,34] The background was fitted using a linear interpolation between selected positions in 2θ. The pseudo-Voigt profile function proposed by Thompson et al. was used to fit the observed peak shape.[35] To reduce the number of parameters, isotropic displacement factors were restrained to be the same for all the atoms. Geometrical soft restraints on the T−O (T = Si, Al) and O−O bond distances within tetrahedra were applied: the distances between Si−O and Al−O were restrained to target values of 1.620 ± 0.001 Å and 1.750 ± 0.001 Å, respectively, and the O−O distances to 2.646 ± 0.005 Å for the Si tetrahedra and 2.858 ± 0.005 Å for the Al tetrahedra. The water molecules were modeled using only the oxygen position and an oxygen scattering factor. In the final stages of the refinements, we refined simultaneously all profile parameters, the scale factor, the lattice constants, a 2θ zero shift, as well as the atomic positional and displacement parameters. The refined crystallographic parameters are summarized in Table 1, and selected bond distances and angles are listed in Table 2. Temperature-dependent structural changes of superhydrated natrolite at 1.76(3) GPa and natrolite at ambient pressure indicate that treating these materials as rotating rigid units is a valid approximation (see Tables 1 and 2 and Figure 1).

RESULTS AND DISCUSSION

The temperature-dependent changes of the orthorhombic unit cell parameters of superhydrated natrolite at 1.7(3) GPa reveal a positive thermal expansion of the *a*- and *b*-unit cell axes, while the *c*-axis reveals a negative thermal expansion (Figure 2 and Table 1). The magnitude and anisotropy of the thermal expansion of superhydrated natrolite are larger than those observed in natrolite at ambient pressure.[10,13] In particular, the average linear coefficient of thermal expansion of the *a*-unit cell axis of superhydrated natrolite, $\alpha^s_a = 4.6 \times 10^{-4}$ K, is about 6.5 times larger than that of natrolite, $\alpha^o_a = 7.1 \times 10^{-5}$ K^{-1} between 20 and 300 K (Figure 2a). The *a*- and *b*-unit cell axes of natrolite contract only marginally under ambient pressure conditions when cooled to 20 K as shown in Figures 2a and 2b. However, in the superhydrated natrolite phase a significant enhancement of the contraction of the *a*-unit cell axis when lowering the temperature is observed. The Rietveld refinements reveal that this goes hand in hand with changes in the sodium−water substructure located in the micropores: as the chain rotation angle ψ increases from 23.8(1)° at 300 K to 24.3(1)° at 20 K and the eight-ring window becomes more elliptical, the oxygen−oxygen distance between the type-1 water (OW1) and the framework O(1) atom increases from 2.84(3) to 2.94(3) Å, while the distance to the other framework oxygen O(5) atom remains constant within the errors of the Rietveld refinement (Table 2). At the same time, when lowering the temperature from 300 to 20 K in the superhydrated phase, the distance of the oxygen of the type-2 water inserted during PIH (OW2) to the framework oxygen O(3) decreases from 2.90(2) to 2.77(2) Å. This shorter distance at 20 K will strengthen the hydrogen bonding to the framework oxygen. The larger-scale structural changes can best be described by two oxygen−oxygen vectors of the two different crystal waters: a type-1 OW1−OW1 vector along the shorter (minor) axis of the (elliptical) eight-ring window and the perpendicular type-2 OW2−OW2 vector along the larger (major) axis (see Figures 1a and b). The two oxygen atoms of the two type-2 water molecules are located along the major axis of the elliptical window forming an angle of 46.9(1)° to the *a*-axis and 43.2(1)° to the *b*-axis. When cooling from 300 to 20 K at 1.76(3) GPa, the OW1−OW1 distance decreases from 4.84(3) to 4.68(3) Å, while the OW2−OW2 distance increases from 4.94(3) to 5.14(3) Å. A concomitant increase of the distance of the sodium ion to the oxygen of OW2 from 2.40(2) to 2.51(2) Å will even further enhance the under-bonding of this type-2 water at 20 K.

The thermal expansion of the *b*-unit cell length of superhydrated natrolite reveals that the average linear

Table 2. Selected Interatomic Distances (Å) and Angles (°) for the Superhydrated Natrolite at 1.76 GPa and Different Temperatures[a]

	1.76 GPa, 20 K	1.76 GPa, 100 K	1.76 GPa, 200 K	1.76 GPa, 300 K
Si(1)−O(1)	1.620(1)	1.621(2)	1.620(1)	1.620(1)
Si(1)−O(5)	1.620(1)	1.621(2)	1.619(1)	1.620(1)
mean[b]	1.620(1)	1.621(1)	1.620(1)	1.620(1)
Si(2)−O(2)	1.620(1)	1.618(2)	1.618(2)	1.619(2)
Si(2)−O(3)	1.620(1)	1.622(2)	1.620(2)	1.620(2)
Si(2)−O(4)	1.620(1)	1.620(2)	1.619(2)	1.620(2)
Si(2)−O(5)	1.620(1)	1.622(2)	1.621(2)	1.620(2)
mean[b]	1.620(1)	1.621(1)	1.620(1)	1.620(1)
Al−O(1)	1.750(1)	1.753(2)	1.751(2)	1.751(2)
Al−O(2)	1.750(1)	1.748(2)	1.749(2)	1.749(2)
Al−O(3)	1.750(1)	1.750(2)	1.749(2)	1.750(2)
Al−O(4)	1.750(1)	1.751(2)	1.750(2)	1.750(2)
mean[b]	1.750(1)	1.751(1)	1.750(1)	1.750(1)
Si(1)−O(1)−Al	141.7(2)	140.9(5)	140.6(5)	141.6(4)
Si(2)−O(2)−Al	128.0(2)	126.2(4)	127.6(4)	128.6(3)
Si(2)−O(3)−Al	136.4(3)	136.8(6)	136.7(6)	137.9(5)
Si(2)−O(4)−Al	137.8(3)	137.5(6)	138.0(6)	136.1(5)
Si(1)−O(5)−Si(2)	144.0(3)	143.8(5)	144.4(5)	144.4(4)
Av. chain rotation angle, ψ	24.3(1)	24.1(1)	24.0(1)	23.8(1)
Na−O(2)	2.49(2)	2.48(2)	2.47(2)	2.54(2)
	2.49(2)	2.53(2)	2.54(2)	2.50(2)
Na−O(3)	2.63(2)	2.61(2)	2.60(1)	2.60(1)
Na−O(4)	2.86(2)	2.81(2)	2.83(2)	2.82(2)
Na−OW1	2.27(3)	2.30(3)	2.39(3)	2.45(3)
	2.52(3)	2.51(3)	2.48(3)	2.52(3)
Na−OW2	2.51(2)	2.47(2)	2.51(2)	2.40(2)
OW1−O(1)	2.94(3)	2.94(3)	2.87(3)	2.84(3)
OW1−O(5)	2.96(3)	2.97(3)	2.96(3)	2.98(3)
OW2−O(1)	2.97(2)	3.03(3)	2.98(2)	2.98(2)
			2.96(2)	
OW2−O(3)	2.77(2)	2.78(2)	2.87(2)	2.90(2)
OW2−O(4)	2.80(2)	2.83(2)	2.75(2)	2.78(2)
OW1−OW2	2.91(2)	2.95(2)	2.86(2)	2.95(2)

[a]Esd's are in parentheses. [b]Standard deviations computed using $\sigma = 1/n[\Sigma_{i=1}^{n}\sigma_i^2]^{1/2}$.

dx.doi.org/10.1021/jp209514q | J. Phys. Chem. C 2012, 116, 3286−3291

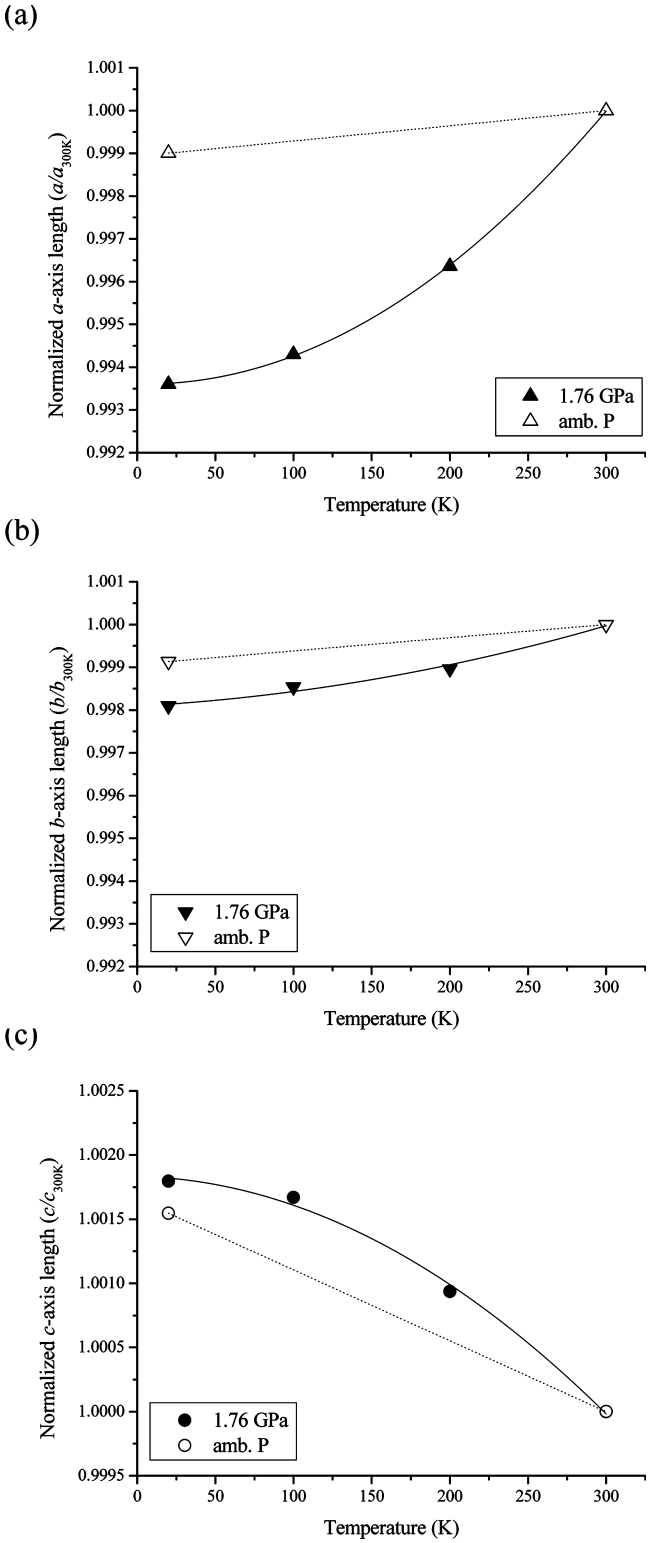

Figure 2. Temperature-dependent changes of the orthorhombic unit cell edge lengths (Å) of the superhydrated natrolite phase formed at 1.7(3) GPa. Estimated standard deviations (esd's) are smaller than each symbol. For comparison, the unit cell lengths of the original natrolite at ambient pressure are shown as open symbols.

coefficient of thermal expansion is ca. 2.3 times larger between 20 and 300 K, $\alpha^s_b = 1.4 \times 10^{-4}$ K^{-1}, than the one measured in natrolite at ambient conditions, $\alpha^o_b = 6.2 \times 10^{-5}$ K^{-1} (Figure 2b). Accordingly, the anisotropy of the average linear thermal expansion of the *a*- and *b*-unit cell lengths is about 3 times larger in the superhydrated natrolite, i.e., $\alpha^s_a:\alpha^s_b = 3.3:1$, than in the natrolite at ambient conditions, i.e., $\alpha^o_a:\alpha^o_b = 1.1:1$. On the other hand, the *c*-unit cell lengths of superhydrated natrolite and natrolite at ambient pressure exhibit very similar magnitudes of negative thermal expansion (Figure 2c). Between 20 and 300 K, the average linear coefficients of thermal expansion along the *c*-unit cell direction are $\alpha^s_c = -1.3 \times 10^{-4}$ K^{-1} and $\alpha^o_c = -1.1 \times 10^{-4}$ K^{-1} for superhydrated natrolite and natrolite at ambient pressure, respectively. Overall, the thermal unit cell volume expansion coefficient of superhydrated natrolite between 20 and 300 K is ca. 15 times larger than that of natrolite at ambient pressure, i.e., $\beta^o = 3.1 \times 10^{-5}$ K^{-1} and $\beta^s = 4.7 \times 10^{-4}$ K^{-1} (Figure 3).

As outlined above, changes in the framework geometry can be monitored by examining the ellipticity of the eight-ring channels in the *ab*-plane (see Figure 1c). Cooling in the superhydrated phase leads to an increase of the chain rotation angle, ψ (Figure 3), and thus an increase of the ellipticity of the eight-ring channels. The sodium water substructure adapts to this distortion by shortening the distances between type-1 water molecules and elongating the ones between the type-2 water molecules. One can formally define a temperature-dependent distortion angle by $\gamma\psi = (\psi_{300} - \psi_{20})/[\psi_{20}(T_{300} - T_{20})]$ with the subscripts of the angle and temperature denoting the temperature in K. The average "angular" coefficient of thermal expansion for the chain rotation angle ψ of superhydrated natrolite under 1.7(3) GPa pressure is $\gamma^s_\psi = -6.6(1) \times 10^{-5}$ K^{-1}. The corresponding value for natrolite at ambient pressure is $\gamma^o_\psi = -7.9(1) \times 10^{-5}$ K^{-1}.[10,13] The ratio $-\gamma/\beta$ of the negative value of this angular expansion coefficient γ and the unit cell volume expansion coefficients β can be used to gauge the impact of the T_5O_{10} rotation angle on the unit cell volume. For superhydrated natrolite at 1.7(3) GPa, $-\gamma/\beta$ is ca. 0.14, whereas it is ca. 2.5 for natrolite at ambient pressure. The channel opening per volume change is thus larger in natrolite at ambient pressure than in superhydrated natrolite. In other words, the smaller thermal expansion in natrolite at ambient pressure leads to a much larger increase of the pore opening. Lethbridge et al.[28] demonstrated, using molecular mechanics simulations, that the presence of nonframework cations and water molecules in the pores of an aluminosilicate framework suppresses the magnitude of auxetic behavior compared to a hypothetical siliceous one. However, natrolite with an aluminosilicate framework was found to be an auxetic material at ambient conditions.[26] Nevertheless the "stuffing" of this framework with extra framework cations and water will reduce the magnitude of its auxetic properties by hindering the rotations of the T_5O_{10} subunits. The above proposed parameter $-\gamma/\beta$ might be a good metric for this behavior.

In summary, using combined in situ high-pressure, low-temperature synchrotron powder diffraction we have measured and structurally characterized the thermal expansion of superhydrated natrolite. Compared to natrolite at ambient pressure, the average linear coefficients of thermal expansion and their anisotropy are larger in superhydrated natrolite, resulting in a 15-fold increase of the thermal volumetric expansion coefficient. The higher packing efficiency at low temperatures in superhydrated natrolite is largely due to changes in the environment of the newly formed sodium–water substructure during pressure-induced hydration. We hope that our results will be useful for the growing modeling efforts

dx.doi.org/10.1021/jp209514q | J. Phys. Chem. C 2012, 116, 3286–3291

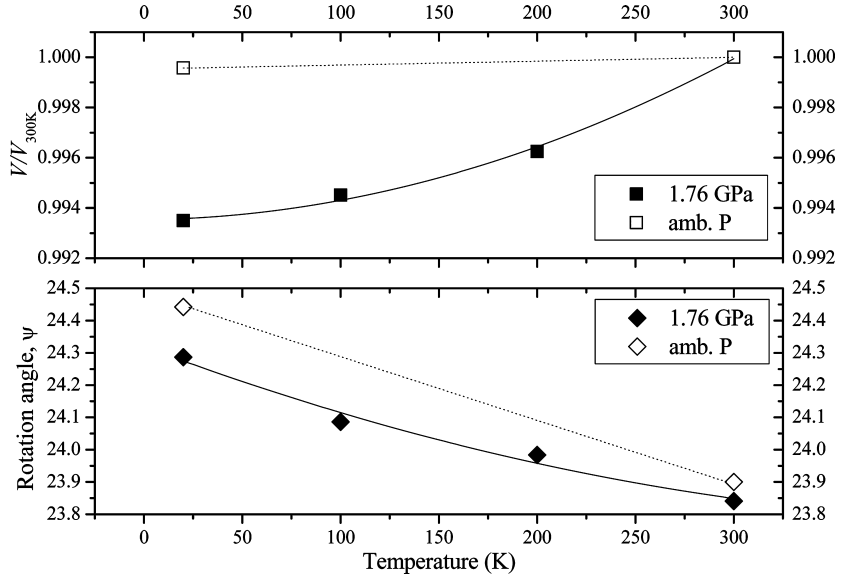

Figure 3. Temperature-dependent changes of (a) the unit cell volume (Å^3) and (b) and the overall chain rotation angle of the superhydrated natrolite formed at 1.7(3) GPa. For comparison, the corresponding values of the original natrolite at ambient pressure are shown as open symbols.

directed at understanding the auxetic behavior of natrolite and other systems.

AUTHOR INFORMATION

Corresponding Author

*E-mail: yongjaelee@yonsei.ac.kr. Tel.: +82-2-2123-5667. Fax: +82-2-2123-8169.

ACKNOWLEDGMENTS

This work was supported by the Global Research Laboratory Program of the Korean Ministry of Education, Science and Technology (MEST). The NSLS at BNL is supported by the U.S. Department of Energy, Office of Basic Energy Sciences.

REFERENCES

(1) Belitsky, I. A.; Fursenko, B. A.; Gubada, S. P.; Kholdeev, O. V.; Seryotkin, Y. V. *Phys. Chem. Miner.* **1992**, *18*, 497.
(2) Lee, Y.; Hriljac, J. A.; Kim, S. J.; Hanson, J. C.; Vogt, T. *J. Am. Chem. Soc.* **2003**, *125*, 6036.
(3) Lee, Y.; Hriljac, J. A.; Parise, J. B.; Vogt, T. *Am. Mineral.* **2005**, *90*, 252.
(4) Lee, Y.; Vogt, T.; Hriljac, J. A.; Parise, J. B.; Artioli, G. *J. Am. Chem. Soc.* **2002**, *124*, 5466.
(5) Lee, Y.; Vogt, T.; Hriljac, J. A.; Parise, J. B.; Hanson, J. C.; Kim, S. J. *Nature* **2002**, *420*, 485.
(6) Hill, G. L.; Bailey, E.; Stennett, M. C.; Hyatt, N. C.; Maddrell, E. M.; McMillan, P. F.; Hriljac, J. A. *J. Am. Chem. Soc.* **2011**, *133*, 13883.
(7) Loewenstein, W. *Am. Mineral.* **1942**, *39*, 92.
(8) Meier, W. M. *Z. Kristallogr.* **1960**, *113*, 430.
(9) Pauling, L. *Proc. Nat. Acad. Sci.* **1930**, *16*, 453.
(10) Baur, W. H.; Kassner, D.; Kim, C.-H.; Sieber, N. H. *Eur. J. Mineral* **1990**, *2*, 761.
(11) Lee, Y.; Hriljac, J. A.; Vogt, T. *J. Phys. Chem. C* **2010**, *114*, 6922.
(12) Lee, Y.; Liu, D.; Seoung, D.; Liu, Z.; Kao, C.-C.; Vogt, T. *J. Am. Chem. Soc.* **2011**, *133*, 1674.
(13) Artioli, G.; Smith, J. V.; Kvick, A. *Acta Crystallogr.* **1984**, *C40*, 1658.
(14) Kolesov, B. A.; Geiger, C. A. *Am. Mineral.* **2006**, *91*, 1039.
(15) Seryotkin, Y. V.; Bakakin, V. V.; Fursenko, B. A.; Belitsky, I. A.; Joswig, W.; Radaelli, P. G. *Eur. J. Mineral.* **2005**, *17*, 305.
(16) Colligan, M.; Lee, Y.; Vogt, T.; Celestian, A. J.; Parise, J. B.; Marshall, W. G.; Hriljac, J. A. *J. Phys. Chem. B* **2005**, *109*, 18223.
(17) Lee, Y.; Martin, C. D.; Parise, J. B.; Hriljac, J. A.; Vogt, T. *Nano Lett.* **2004**, *4*, 619.
(18) Lee, Y.; Hriljac, J. A.; Parise, J. B.; Vogt, T. *Am. Mineral.* **2006**, *91*, 247.
(19) Lee, Y.; Seoung, D.; Bai, J.; Kao, C.-C.; Parise, J. B.; Vogt, T. *J. Phys. Chem. C* **2010**, *114*, 18805.
(20) Baur, W. H. *J. Solid State Chem.* **1992**, *97*, 243.
(21) Baur, W. H.; Joswig, W.; Müller, G. *J. Solid State Chem.* **1996**, *121*, 12.
(22) Grima, J. N.; Farrugia, P. S.; Caruana, C.; Gatt, R.; Attard, D. *J. Mater. Sci.* **2008**, *43*, 5962.
(23) Grima, J. N.; Jackson, R.; Alderson, A.; Evans, K. E. *Adv. Mater.* **2000**, *12*, 1912.
(24) Love, A. E. H. *A treatise on the mathematical theory of elasticity*, 4 ed.; Dover: New York, 1944.
(25) Evans, K. E.; Nkansah, M. A.; Hutchison, I. J.; Rogers, S. C. *Nature* **1991**, *353*, 124.
(26) Grima, J. N.; Gatt, R.; Zammit, V.; Williams, J. J.; Evans, K. E.; Alderson, A.; Walton, R. I. *J. Appl. Phys.* **2007**, *101*, 086102.
(27) Grima, J. N.; Gatt, R.; Ellul, B.; Chetcuti, E. *J. Non-Cryst. Solids* **2010**, *356*, 1980.
(28) Lethbridge, Z. A. D.; Williams, J. J.; Walton, R. I.; Smith, C. W.; Hooper, R. M.; Evans, K. E. *Acta Mater.* **2006**, *54*, 2533.
(29) Smith, G. C. *Synchrotron Radiat. News* **1991**, *4*, 24.
(30) Merrill, L.; Bassett, W. A. *Rev. Sci. Instrum.* **1974**, *45*, 290.
(31) Mao, H. K.; Hemley, R. J. *Phil. Trans. R. Soc. London A* **1996**, *354*, 1315.
(32) Angel, R. J. In *Reviews in Mineralogy and Geochemistry: High-Temperature and High-Pressure Crystal Chemistry*; Hazen, R. M., Downs, R. T., Eds.; The Mineralogical Society of America: Washington, DC, 2000; Vol. *41*, p 35.
(33) Larson, A. C.; VonDreele, R. B. *GSAS; General Structure Analysis System*, Report LAUR 86−748, Los Alamos National Laboratory: NM, 1986.
(34) Toby, B. H. *J. Appl. Crystallogr.* **2001**, *34*, 210.
(35) Thompson, P.; Cox, D. E.; Hastings, J. B. *J. Appl. Crystallogr.* **1987**, *20*, 79.